Analysis of Zone-Drawing Process in Preoriented Polypropylene

K. YAMADA and M. TAKAYANAGI, *Department of Applied Chemistry, Faculty of Engineering, Kyushu University, Fukuoka 812, Japan*

Synopsis

Preoriented isotactic polypropylene was used to clarify the molecular process in zone-drawing with which the necking part is confined in a thin heating zone during uniaxial drawing. The process was analyzed on the basis of rate process, the mechanical properties of zone-drawn samples, and the superstructural change during zone-drawing. The values of activation energy for deformation, ΔH^*, and the activation volume, ΔV^*, were affected by the deformation mechanisms preferentially taking place during the zone-drawing. The attainable maximum modulus of zone-drawn sample at $\theta = 45°$ was larger than those at $\theta = 0°$ and 90°. The highest strength was also obtained at $\theta = 45°$. The values of modulus and strength strongly depended on both the orientation function of the crystal c-axis and the orientation function of amorphous chains. In the region of a very high zone-drawing rate, in which microcracks are preferentially formed, both modulus and strength decreased, whereas they increased with increasing the zone-drawing rate below this region, giving the optimum condition for achieving the maxima in the modulus and strength.

INTRODUCTION

The effects of the molecular aggregation state of polymers on drawing behavior have been investigated by several authors.[1–3] Capaccio et al.[1] reported the influence of the degree of crystallinity and morphology on the drawing behavior of linear polyethylene. The drawing process was not dominantly affected by crystallinity, but the morphology was an influential factor as detected by optical microscopy. Mead and Porter[2] obtained ultraoriented polyethylene fibers by solid-state extrusion from various isothermally crystallized morphologies. Maximum birefringence was obtained with increasing crystallization temperature and molecular weight. Kanamoto et al.[3] studied the solid-state extrusion of both unoriented polyethylene single-crystal aggregates and melt-crystallized polyethylene. The initial morphologies had no appreciable effect on the modulus for the samples prepared with various area reduction in extrusion, but the maximum attainable modulus was higher for the single-crystal aggregates than for the spherulitic samples.

In our previous work[4–6] a superstructural change of preoriented crystalline polymers during uniaxial drawing was investigated by means of X-ray goniometry. The angles θ between the drawing direction and the crystal c-axis of the preoriented polymer were varied from 0° to 90°. The strain on uniaxial extension of preoriented isotactic polypropylene was separated over the whole range of deformation into three processes: crystallite boundary slip (A_1 process), uniform shear deformation of crystallites (A_2 process), and restoration of molecular orientation from the shear-deformed state ($\overline{A_2}$ process). The last process was presumed to take place owing to the reconstruction of the superstructure once destructed. They were separately evaluated by the use of the parameters of

Journal of Applied Polymer Science, Vol. 27, 2091–2103 (1982)
 CCC 0021-8995/82/062091-13$02.30

superstructure, which varied in the deformation. Such a superstructural change during drawing significantly depended on the drawing direction θ. The superstructural analysis of plastic deformation of crystalline polymers can be more briefly done by using a preoriented sample with uniaxial orientation than by a bulk-crystallized sample with statistically random orientation. The increase of the orientation function of amorphous chains, f_a, with extension of preoriented isotactic polypropylene also depended on the testing direction θ.[7] The f_a most effectively increased in extension at $\theta = 45°$. For the uniaxially oriented isotactic polypropylene prepared from the bulk-crystallized specimen by the forced-quenching-type zone-drawing apparatus equipped with a local heating furnace, the increase of modulus at a high draw ratio is caused by the increase of the fraction of taut tie molecules associated with the increase of orientation function of amorphous chains.[8]

On the other hand, to analyze the drawing process, Pechhold[9] and Davis and Pampillo[10] introduced a rate-controlling mechanism. Pechhold[9] explained the temperature and strain dependence of the yield stress in a melt-crystallized linear polyethylene. His model is based on the motion of dislocations within the crystal lamellae. Davis and Pampillo[10] measured the yield stress and the flow stress at different strains as a function of temperature for a melt-crystallized linear polyethylene. Two transitions were found on the flow stress at about 175 K and 265 K. Only one transition at about 170 K was found on the yield stress. Such transitions were assigned to a change in the rate of peroxy radical accumulation determined by electron paramagnetic resonance spectroscopy.[11]

In the zone-drawing, the deformation of the sample is restricted only in the heating zone, different from the usual drawing in air bath by Pechhold[9] and Davis and Pampillo.[10] That is to say, the sample is drawn by the tensile tester and at the same time the ensemble of the heater and cooler is shifted at an appropriate rate so that the deformed region is confined within the heater zone during the drawing. The draw ratio can be controlled by the ratio of the drawing rate of the tensile tester to the shifting rate of the heater–cooler ensemble. Thus the deformation in the heater realizing a high draw ratio will include all deformation processes of the usual drawing, in which necking, propagation of the necking, and then, furthermore, deformation after the end of the necking take place before breaking.

In this work how the zone-drawing process is affected by the testing direction θ is clarified by using preoriented isotactic polypropylene. The zone-drawing process is analyzed on the basis of the rate process, the mechanical properties of zone-drawn samples, and the superstructural change during zone-drawing, taking into account the results of previous works.[5–7] Such analyses of zone-drawing process are effective in preparation of a uniaxially oriented crystalline polymer with high modulus by means of the zone-drawing.

EXPERIMENTAL

Sample Preparation with Zone-Drawing Method

The sample used was isotactic polypropylene, MA-8 (Mitsubishi Yuka Co., Ltd.), the viscosity-average molecular weight of which was 510,000. The pellets of MA-8 were compression-molded at 493 K between two brass plates in a ni-

trogen atmosphere to give a sheet about 0.8 mm thick, which was rapidly quenched by plunging it into ice water. The preoriented sample, about 0.2 mm thick, having a uniaxially oriented structure, was prepared by drawing the quenched sheet at 393 K with draw ratio of about 7.6. The drawing speed was 5 mm/min for the gauge length of 70 mm. The specimens 1 mm wide for the purpose of zone-drawing were cut out from the preoriented sample in such a way that the angles between the zone-drawing direction and the crystal c-axis, θ, were 0°, 45°, and 90°. A tensile tester, Tensilon UTM-III (Toyo Baldwin Co., Ltd.) equipped with the ensemble of heater and cooler, as shown in Figure 1(a) was employed. The forced quenching type zone-drawing part is illustrated in Figure 1(b). The heater temperature was varied from 390 K to 410 K, and the cooler temperature was 263 K. The raising speed of the ensemble of heater and cooler was 16 mm/min, and the drawing speed was in the range of 2–500 mm/min. A draw ratio λ was evaluated from the reduction of the corss-sectional area of the specimen as follows:

$$\lambda = A_0/A$$

where A_0 and A are the cross-sectional areas before and after zone-drawing, respectively. In the case of zone-drawing, the increase of the drawing rate corresponds to the increase of the draw ratio λ. Drawing stress was evaluated by dividing the load by the cross-sectional area of the specimen after zone-drawing.

Measurements of Modulus and Strength

The modulus of a zone-drawn specimen was measured at room temperature with a dynamic viscoelastometer, Rheovibron DDV-II-C (Toyo Baldwin Co., Ltd.), at 3.5 Hz. The absolute value of the complex modulus was taken as the modulus in this work. The complex modulus was evaluated by using the correction factor of displacement given for the dynamic viscoelastometer. Strength (maximum stress) was measured with the gage length of 10 mm at the crosshead

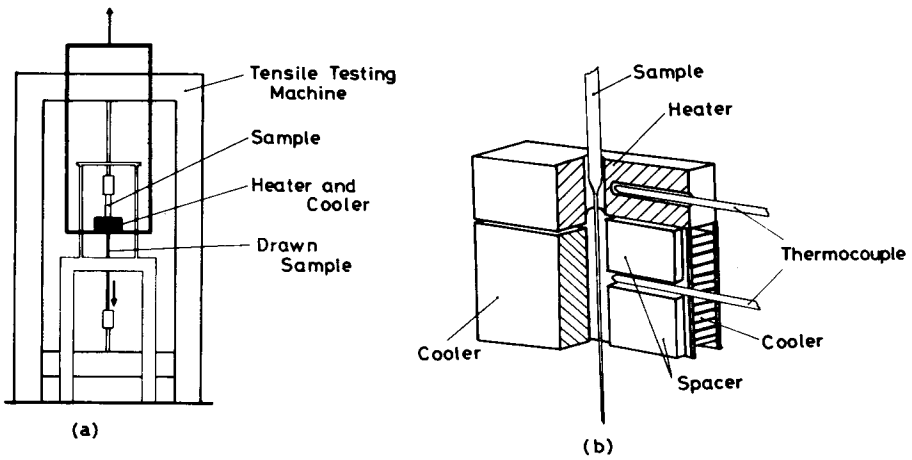

Fig. 1. (a) Schematic representations of forced quenching type zone-drawing apparatus equipped with a tensile tester and (b) the detailed construction of the heater and cooler.

speed of 5 mm/min with a tensile tester, Tensilon UTM-III (Toyo Baldwin Co., Ltd.).

Density, Birefringence, and Orientation Functions of Crystal *c*-Axis and Amorphous Chains

Density was measured at 303 K with a floating method using an ethanol–water mixture. Birefringence was measured at room temperature with a polarization microscope, POH (Nippon Kogaku Co., Ltd.). The orientation function of the crystal *c*-axis, f_c, was evaluated from the azimuthal intensity distributions of X-ray diffraction of the (110) and (040) planes by the usual method. The orientation function of amorphous chains was evaluated by using density, birefringence, and f_c on the assumptions that (1) the form birefringence can be neglected, (2) the intrinsic birefringences of the crystalline and amorphous regions are 0.0285 and 0.0618, respectively,[12] and (3) the densities of crystalline and amorphous regions are 0.933 and 0.853 g/cm^3,[13] respectively.

Measurement of the Angle between Zone-Drawing Direction and Crystal *c*-Axis after Zone-Drawing

The x-ray beam was irradiated perpendicular to the zone-drawing direction of the sample, and the azimuthal intensity distribution of (110) diffraction was measured. The zone-drawing direction was parallel to the meridional direction. The azimuthal angle of maximum intensity points of (110) measured from the meridional direction corresponds to the value of $(90° - \phi)$. Such an azimuthal angle ϕ agreed with that of the (040) diffraction.

RESULTS

Analysis of Zone-Drawing Process from the Viewpoints of Rate Process

Figure 2 shows σ_n/T_d as a function of zone-drawing rate for $\theta = 0°$ at the heater temperatures T_d = 390 K, 400 K, and 410 K, where σ_n is zone-drawing stress.

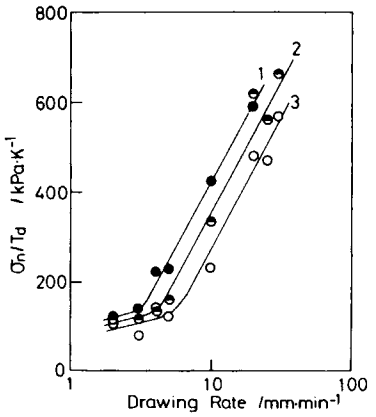

Fig. 2. Ratio of zone-drawing stress (σ_n) to heater temperature (T_d), σ_n/T_d, as a function of zone-drawing rate for $\theta = 0°$ at T_d = 390 K(1), 400 K(2), and 410 K(3).

The linear relationship between σ_n/T_d and the common logarithm of the zone-drawing rate holds in the region of zone-drawing rates of 5–30 mm/min. Perhaps another linear relationship might hold below 2–5 mm/min. The slopes of these straight lines differ from each other. Such a linear relationship was also valid in the regions of lower and higher rates for $\theta = 45°$ and 90°. The zone-drawing rates at the crossing points of the two straight lines were equal to about 100 mm/min, for both the cases of $\theta = 45°$ and 90°. Since the sample was deformed in the heater during the zone-drawing, the zone-drawing rate was proportional to the average strain rate $\dot{e}$ under the conditions of regulating the shifting rate of the heater to the value of 16 mm/min. This average strain rate, therefore, corresponds to the average rate of necking formation, which determines the drawn ratio. The average strain rate $\dot{e}$ at zone-drawing stress σ_n may be represented by the following equation[10]:

$$\dot{e} = A \exp(-\Delta H^*/kT_d) \tag{1}$$

$$= A \exp[-(\Delta H_0^* - \Delta V^* \sigma_n)/kT_d] \tag{2}$$

where A is a constant, ΔH^* the apparent activation energy, k Boltzmann's constant, ΔV^* the activation volume, σ_n zone-drawing stress, and ΔH_0^* the activation energy at $\sigma_n = 0$ MPa. Equation (1) leads to the following equation:

$$\Delta H^* = -\left(\frac{\partial \ln \dot{e}}{\partial(1/kT_d)}\right)_{\sigma_n,e} = kT_d^2 \left(\frac{\partial \ln \dot{e}}{\partial \ln \sigma_n}\right)_{T_d,e} \left(\frac{\partial \ln \sigma_n}{\partial T_d}\right)_{\dot{e},e} \tag{3}$$

where e is strain; from eq (2),

$$\Delta V^* = \frac{kT_d}{\sigma_n} \left(\frac{\partial \ln \dot{e}}{\partial \ln \sigma_n}\right)_{T_d,e} \tag{4}$$

Relationship between ΔH^* and Zone-Drawing Rate

Figure 3 shows ΔH^*, which was evaluated by using both eq. (3) and the σ_n/T_d versus zone-drawing rate curves at $T_d = 400$ K and 410 K, as a function of the zone-drawing rate for $\theta = 0°$, 45°, and 90° at $T_d = 405$ K. The zone-drawing rate is hereafter represented by $\dot{d}$. In each testing condition the value of the apparent activation energy in the region of higher $\dot{d}$, ΔH_h^*, became always lower than that in the region of lower $\dot{d}$, ΔH_l^*. The values of ΔH_l^* for $\theta = 0°$, 45°, and

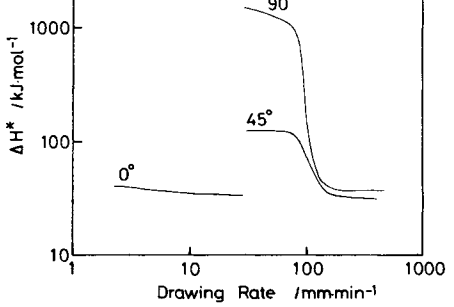

Fig. 3. Apparent activation energy, ΔH^*, as a function of zone-drawing rate for $\theta = 0°$, 45°, and 90° at $T_d = 405$ K.

90° were about 40 kJ/mol, 130 kJ/mol, and 1200 kJ/mol, respectively, whereas those of ΔH_h^* for $\theta = 0°$, 45°, and 90° were about 34 kJ/mol, 32 kJ/mol, and 38 kJ/mol, respectively. This fact shows that the deformation mechanisms in the regions of lower and higher zone-drawing rates differ from each other. Such a difference in the value of ΔH^* became larger with increasing θ. At the region of lower $\dot{d}$, the value of ΔH^* at higher θ was larger than that at lower θ, whereas at the region of higher $\dot{d}$ the values of ΔH^* at each θ are approximately equal to each other, independent of θ. This fact shows that the deformation mechanism in the region of lower $\dot{d}$ is considerably dependent on the testing direction θ, whereas that in the region of higher $\dot{d}$ is almost independent of θ. These results will be discussed in a later part.

Relationship between Activation Volume and Zone-Drawing Rate

Figure 4 shows the activation volume ΔV^* as a function of the zone-drawing rate $\dot{d}$, in the same testing conditions as in Figure 3. ΔV^* at the lower $\dot{d}$ was always larger than that at higher $\dot{d}$. Furthermore, the ΔV^* *versus* $\dot{d}$ curve was shifted to the higher ΔV^* with increasing θ in all range of $\dot{d}$. The value of ΔV^* may be used as a measure of the size of the deformation unit, based on the assumption that the zone-drawing stress uniformly acts on all the deformation units. According to such an idea, the deformation unit has a smaller size in the region of higher $\dot{d}$ and at a lower value of θ.

Mechanical Properties of Zone-Drawn Samples

Modulus vs. Zone-Drawing Rate Curve

Figure 5 shows the modulus of a zone-drawn sample as a function of the zone-drawing rate $\dot{d}$ for $\theta = 0°$, 45°, and 90° at $T_d = 410$ K. In our previous work,[14] it was found that the maximum modulus was obtained at $T_d = 410$ K by employing bulk-crystallized polypropylene. Thus, $T_d = 410$ K was used this

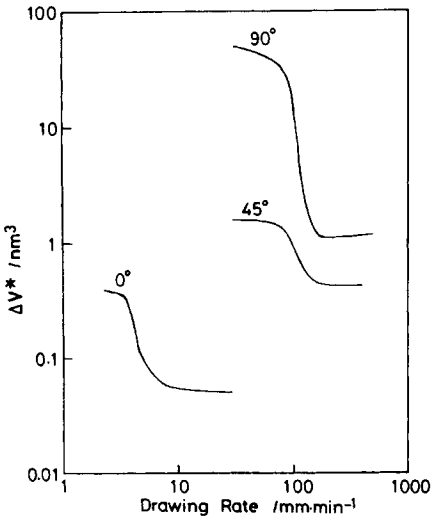

Fig. 4. Activation volume, ΔV^*, as a function of zone-drawing rate in the same testing conditions as in Figure 3.

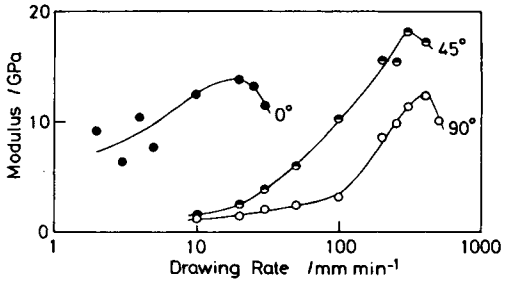

Fig. 5. Modulus as a function of zone-drawing rate for $\theta = 0°$, 45°, and 90° at $T_d = 410$ K.

time. The modulus increased with $\dot{d}$, but decreased above high $\dot{d}$ after taking the maximum. In these zone-drawing conditions the attainable maximum moduli at $\theta = 0°$, 45°, and 90° were 14 GPa, 18 GPa, and 12 GPa, respectively. The zone-drawing rates at maximum moduli were 20 mm/min at $\theta = 0°$, 300 mm/min at $\theta = 45°$, and 400 mm/min at $\theta = 90°$. It was found that $\theta = 45°$ is the best for achieving the highest modulus.

Modulus vs. Zone-Drawing Stress Curve

Figure 6 shows the modulus as a function of zone-drawing stress σ_n at $\theta = 0°$, 45°, and 90° and $T_d = 410$ K. At each testing direction, the modulus largely increased with increasing σ_n in the region of lower σ_n, but decreased or slightly increased in the region of higher σ_n. At $\theta = 45°$, both the highest modulus and the drawing stress were attained.

Strength vs. Zone-Drawing Rate Curve

Figure 7 shows strength as a function of $\dot{d}$ for $\theta = 0°$, 45°, and 90° at $T_d = 410$ K. At each θ, the shape of the strength *versus* $\dot{d}$ curve was very similar to the modulus versus the $\dot{d}$ curve shown in Figure 5. That is to say, strength increased with $\dot{d}$, but decreased above higher $\dot{d}$. The highest strength was obtained at $\theta = 45°$. The $\dot{d}$ at maximum strength for $\theta = 0°$, 45°, and 90° were 20 mm/min, 300 mm/min, and 400 mm/min, respectively. The highest strength was 0.6 GPa.

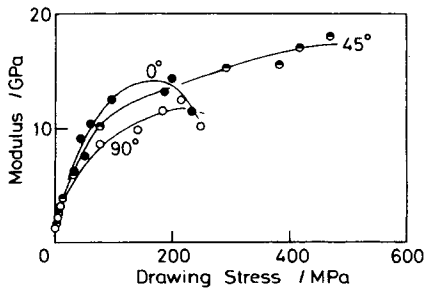

Fig. 6. Modulus as a function of zone-drawing stress for $\theta = 0°$, 45°, and 90° at $T_d = 410$ K.

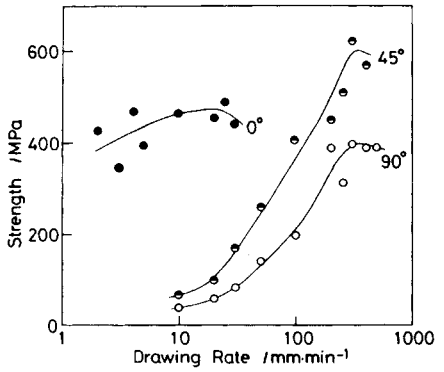

Fig. 7. Strength as a function of zone-drawing rate for $\theta = 0°$, 45°, and 90° at $T_d = 410$ K.

Superstructural Change during Zone-Drawing

Density vs. Zone-Drawing Rate Curve

Figure 8 shows the density as a function of $\dot{d}$ for $\theta = 0°$, 45°, and 90° at $T_d = 410$ K. The density slightly decreased with increasing $\dot{d}$, but largely decreased in the region of higher $\dot{d}$. The values of the $\dot{d}$, at which the density starts to decrease were about 20 mm/min for $\theta = 0°$, 250 mm/min for $\theta = 45°$, and 250 mm/min for $\theta = 90°$. These values of the $\dot{d}$ were almost in agreement with the values of $\dot{d}$ at which the modulus and strength approximately attained maximum values, as shown in Figures 5 and 7.

f_c *vs. Zone-Drawing Rate Curve and* f_a *vs. Zone-Drawing Rate Curve*

Figures 9(a) and (b) show the orientation function of the crystal c-axis, f_c, and the orientation function of amorphous chains, f_a, respectively, as a function of $\dot{d}$ for $\theta = 0°$, 45°, and 90° at $T_d = 410$ K. The value of f_c increased with increasing $\dot{d}$, but scarcely increased or decreased in the region of higher $\dot{d}$. Such a region corresponded to that of $\dot{d}$ in which the modulus and strength decreased with increasing $\dot{d}$ after taking the maxima of the modulus and strength. The maximum f_c was 0.99 at each testing direction.

The value of f_a also increased with $\dot{d}$, but decreased in the same region of the higher zone-drawing rate as in f_c. The maximum value of f_a at $\theta = 45°$ was the largest one among the values at each θ.

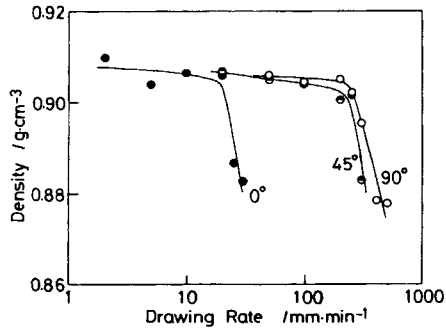

Fig. 8. Density as a function of zone-drawing rate for $\theta = 0°$, 45°, and 90° at $T_d = 410$ K.

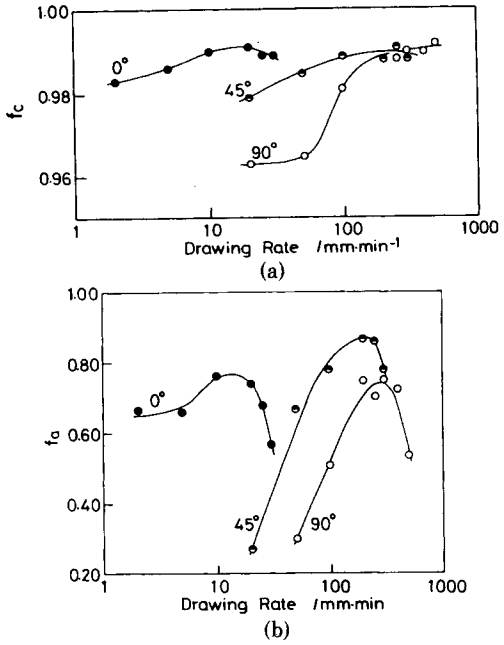

Fig. 9. (a) Orientation function of crystal c-axis and (b) orientation function of amorphous chains as a function of zone-drawing rate for $\theta = 0°$, 45°, and 90° at $T_d = 410$ K.

Draw Ratio vs. Zone-Drawing Rate Curve

Figure 10 shows the draw ratio as a function of $\dot{d}$ for $\theta = 0°$, 45°, and 90° at $T_d = 410$ K. The draw ratio was evaluated from the reduction of the cross-sectional area of a sample. The draw ratio increased with increasing $\dot{d}$, but decreased in the region of higher $\dot{d}$. The decreasing region of the draw ratio approximately agreed with that of the decrease of density, f_c and f_a.

DISCUSSION

According to the previous work,[4–6] the strain on the uniaxial drawing of preoriented isotactic polypropylene at $\theta = 45°$ or 90° in an air bath was separated over the whole range of deformation into three processes. As shown in Figure 11, they are (a) the crystallite boundary slip (A_1 process), (b) uniform shear deformation of crystallites (A_2 process), and (c) restoration of molecular orientation from the shear-deformed state ($\overline{A_2}$ process). Both the A_1 and A_2 processes predominate before the $A_2 \rightarrow \overline{A_2}$ transition takes place at the critical true strain.

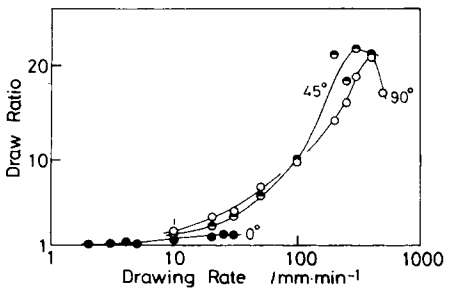

Fig. 10. Draw ratio as a function of zone-drawing rate for $\theta = 0°$, 45°, and 90° at $T_d = 410$ K.

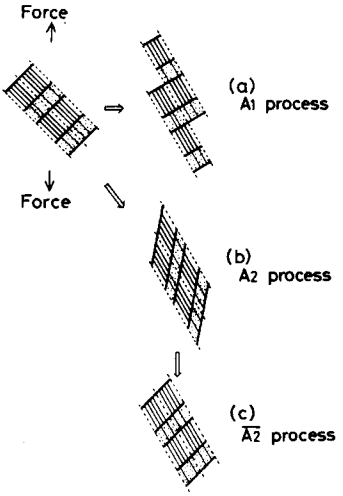

Fig. 11. Schematic representation of three basic types of deformation in uniaxial extension of preoriented polymers: (a) A_1 process, (b) A_2 process, and (c) $\overline{A_2}$ process.

After the $A_2 \rightarrow \overline{A_2}$ transition takes place, the specimen cannot be deformed by the A_1 or A_2 process, but by a molecular process such that the isolated extending chains are pulled out from the folded chain crystals, being followed by their refolding. This molecular process is hereafter termed the regenerating process. The refolding phenomenon is assumed from the fact that the crystallite thickness changed, dependent on the drawing temperature, after the regenerating process took place.[5–7] It is presumed that in the zone-drawing process of the preoriented isotactic polypropylene, the A_1, A_2, and $\overline{A_2}$ processes will take place during necking deformation in a thin heater, with the similar process to that found in the conventional drawing in an air bath as mentioned above.

Figure 12 shows the angle ϕ between the zone-drawing direction and the crystal c-axis after the zone-drawing, as a function of zone-drawing rate $\dot{d}$. At $\theta = 45°$ and 90° the value of ϕ became about 0° above $\dot{d} = 100$ mm/min. The $A_2 \rightarrow \overline{A_2}$ process takes place when ϕ takes the value close to 0° in the conventional drawing in an air bath.[5,6] Therefore, it is presumed that the $A_2 \rightarrow \overline{A_2}$ process will begin to occur in the $\dot{d}$ range below $\dot{d} = 100$ mm/min. At $\dot{d} = 100$ mm/min, the value of the activation energy, ΔH^*, for both cases of $\theta = 45°$ or 90°, largely decreased, as shown in Figure 3. Thus the difference of ΔH^* in the lower and higher $\dot{d}$ regions at $\theta = 45°$ or 90° may originate in the difference in the deformation process.

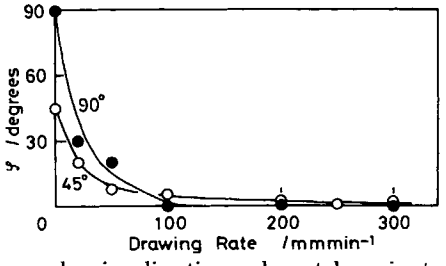

Fig. 12. Angle between zone-drawing direction and crystal c-axis, ϕ, after zone-drawing as a function of zone-drawing rate for $\theta = 45°$ and 90° at $T_d = 410$ K.

In the lower $\dot{d}$ region, the A_1 and A_2 processes preferentially take place, whereas, in the higher $\dot{d}$ region, the regenerating process preferentially takes place. The small difference of ΔH^* in lower $\dot{d}$ and higher $\dot{d}$ regions at $\theta = 0°$ will be discussed later.

From Figures 5 and 9, the increase of modulus corresponds to the increase of both orientation function of the crystal c-axis, f_c, and that of amorphous chains, f_a. The increase of f_a corresponds to the increase of the fraction of taut tie molecules.[8] The taut tie molecules are formed during the regenerating process,[6] which may take place in the range from about 100 mm/min to about 300 mm/min at $\theta = 45°$ or in the range from about 100 mm/min to about 400 mm/min at $\theta = 90°$. However, when $\dot{d}$ increased further above 20 mm/min at $\theta = 0°$, 300 mm/min at $\theta = 45°$, and 400 mm/min at $\theta = 90°$, the modulus decreased with increasing $\dot{d}$. Such a decrease of modulus also well corresponds to the decrease of f_c and f_a. In the $\dot{d}$ region, in which modulus decreased with $\dot{d}$, density more largely decreased (Fig. 8) and the draw ratio evaluated from the reduction of the cross-sectional area also decreased (Fig. 10). It becomes apparent that the f_c, f_a, and an amount of deformation increase to the limit till the density starts to decrease.

The larger decrease of the density at high $\dot{d}$ may originate in the formation of microcracks, which were ascertained by the whitening of the zone-drawn sample. It can be presumed that at high $\dot{d}$, at which the modulus decreases, microcracks are formed and then they grow and/or coalesce with each other. In such situations, f_c and f_a are rather decreased. Figure 13 shows the relationship between the modulus and strength, which is obtained by using Figures 5 and 7. Strength correlates with the modulus. It is a reasonable result, if both the modulus and strength similarly depend on f_c and f_a through taut tie molecules. The modulus and strength depend on the formation of microcracks, which makes both f_c and f_a decrease.

Such microcrack formation process also takes place for $\theta = 0°$ above $\dot{d} = 20$ mm/min as seen in Figures 5, 8, and 9, but, below $\dot{d} = 20$ mm/min, the regenerating process will preferentially take place, since the regenerating process at $\theta = 45°$ and 90° takes place above about 100 mm/min, where the value of ϕ almost attained 0°. However, the activation energy ΔH^* scarcely changed in the whole range of $\dot{d}$ with $\dot{d}$ at $\theta = 0°$, as shown in Figure 3. Therefore, it may be assumed that the value of ΔH^* in the regenerating process is strongly associated with that in the microcrack formation process. The value of ΔH^* in the region of higher $\dot{d}$ at each testing direction, that is, above 2 mm/min at $\theta = 0°$, 100 mm/min at $\theta = 45°$, and 100 mm/min at $\theta = 90°$, is in the range of 30–40 kJ/mol, independent

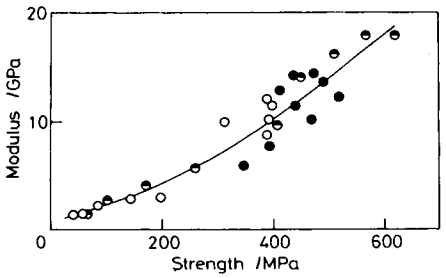

Fig. 13. Modulus as a function of strength for $\theta = 0°$ (●), 45° (◓) and 90° (○) at $T_d = 410$ K.

of the testing direction. It becomes apparent that the activation energy of the regenerating process or microcrack formation process is in the range of 30–40 kJ/mol. The value of activation volume ΔV^* in the A_1 and A_2 processes is in the range of 1–50 nm^3, that in the regenerating process is in the range of 0.4–1 nm^3, and that in the microcrack formation process is around 0.05 nm^3. It becomes apparent from the results of Figure 4 that the size of deformation unit related to the value of ΔV^* is smaller in the regenerating process and the microcrack formation process than that in the A_1 and A_2 processes.

As shown in Figure 5, the testing direction of $\theta = 45°$ gave the highest value of the modulus in the conditions of $\theta = 0°$, 45°, and 90°. As shown in Figure 6, the higher zone-drawing stress at $\theta = 45°$ effectively contributes to increase the modulus without forming microcracks, whereas the increase of the zone-drawing stress at $\theta = 0°$ and 90° does not contribute to obtain a higher modulus, because the breaking of the sample preferentially takes place at the higher zone-drawing stress. Therefore, it is expected that the regenerating process more smoothly takes place at $\theta = 45°$, and then taut tie molecules are more easily formed. Such an increase of the taut tie molecules at $\theta = 45°$ is supported by Fig. 9(b), in which the highest value of f_a can be obtained at $\theta = 45°$. According to the previous works,[5,6] the formation of taut tie molecules in the regenerating process was interpreted as follows: After the folded chains are pulled out of the crystallites by overcoming the intermolecular force to restrain them in the crystallites and conformationally change into extended chains, these extended chains refold to bury the other extended chains, and then the taut tie molecules are newly formed by the formation of the extended chains. In this case the folded chains may be pulled out through both the stretching of tie molecules performed in the original sample and the shearing stress along the crystal c-axis. At $\theta = 45°$ the maximum shearing stress acts along the crystal c-axis in the beginning of extension, whereas at $\theta = 0°$ and 90° the value of the shearing stress is 0. If the shearing stress more effectively acts along the crystal c-axis during extension at $\theta = 45°$, the folded chains are more easily pulled out, and therefore the extended chains are more formed. On the other hand, if at $\theta = 0°$ and 90° the shearing stress does not act effectively in pulling out the folded chains, the preformed tie molecules are more easily broken down through stretching, and the number of the extended chains formed during the regenerating process is decreased. Such a scission of the preformed tie molecules may bring about the formation of the microcracks described previously. Thus the formation of more taut tie molecules at $\theta = 45°$ can be explained by this idea of the regenerating process.

References

1. G. Capaccio, T. A. Crompton, and I. M. Ward, *Polym. Eng. Sci.*, **18**, 533 (1978).
2. W. T. Mead and R. S. Porter, *Int. J. Polym. Mater.*, **7**, 29 (1979).
3. T. Kanamoto, E. S. Sherman, and R. S. Porter, *Polym. J.*, **11**, 497 (1979).
4. K. Yamada and M. Takayanagi, *Kobunshi Ronbunshu*, **34**, 53 (1977).
5. K. Yamada and M. Takayanagi, *Kobunshi Ronbunshu*, **34**, 465 (1977).
6. K. Yamada and M. Takayanagi, *J. Appl. Polym. Sci.*, **24**, 781 (1979).
7. K. Yamada and M. Takayanagi, *J. Appl. Polym. Sci.*, to appear.
8. K. Yamada, M. Kamezawa, and M. Takayanagi, *J. Appl. Polym. Sci.*, **26**, 49 (1981).

9. W. Pechhold, *J. Polym. Sci., Part C*, **32,** 123 (1971).
10. C. A. Pampillo and L. A. Davis, *J. Appl. Phys.*, **43,** 4277 (1972).
11. L. A. Davis and C. A. Pampillo, *J. Polym. Sci., Polym. Phys. Ed.*, **11,** 841 (1973).
12. R. J. Samuels, *J. Polym. Sci., Part C*, **20,** 253 (1967).
13. G. Natta, F. Danusso, and G. Moraglio, Angew. Chem., **69,** 686 (1957).
14. M. Kamezawa, K. Yamada, and M. Takayanagi, *J. Appl. Polym. Sci.*, **24,** 1227 (1979).

Received September 3, 1981
Accepted December 12, 1981